Development of an Age-Specific Finite Element Brain Model to Advance Pediatric Crash Protection

Gabriella Wynn, Matthew B. Panzer

Abstract Motor vehicle crashes are a leading cause of morbidity and mortality among children, with traumatic brain injuries (TBIs) representing a frequent and severe outcome. Finite element (FE) models have been widely used to investigate TBI mechanisms and inform automotive safety measures. However, pediatric FE brain models primarily focus on infants and young children, whereas older children are often represented using adult models that may not produce the same biomechanical response to impact. To address this gap, a new FE pediatric brain model template was developed, and age-specific models representing ages 9 to 14 years were created using Registration-Based Morphing. Age-dependent material properties were incorporated by scaling adult stiffness and damping values using the best available pediatric elastography data. The pediatric and adult models were simulated using 5th percentile female head kinematics from automotive loading conditions. Brain deformation was quantified using maximum principal strain (MPS95) and the cumulative strain damage measure (CSDM15). Differences between the pediatric and adult models were minimal, but the subject-specific comparisons showed stronger, more directionally consistent results, with pediatric subjects having higher regional strain distributions in white matter and adult subjects with higher strains along structural interfaces. This study demonstrated that neuroanatomy variation within this age range contributed to large variation in deformation outcome relative to adults. More investigation is needed before conclusions on pediatric-specific injury risk can be made.

Keywords Computational modelling, Crash biomechanics, Pediatric injury, Traumatic brain injury.

INTRODUCTION

Traumatic brain injuries (TBIs) are a significant source of injury, disability, and death in children. Reported pediatric TBI incidence ranges from 47 to 280 per 100,000 children worldwide. Extrapolated globally, this corresponds to approximately 3 to 17 million cases annually, representing up to 25% of the estimated 69 million TBIs across all ages [1, 2]. Motor vehicle crashes (MVCs) remain a leading cause of death and disability for children, accounting for 20-30% of all TBI-related deaths, despite substantial declines in fatalities over recent decades [3–5]. Among child occupants, the head is the most frequently injured body region across crash directions and restraint types [4], with TBI occurring across a wide range of severities [6]. Children who sustain TBI may develop cognitive, behavioural, and social difficulties, which can be subtle and only become apparent as they grow. Even mild TBI may lead to long-term effects in children. As a result, the consequences of pediatric TBI are often underestimated and may differ from those observed in adults [7].

Finite element (FE) models of the human brain are essential tools for studying TBI. Because injurious motions and resulting tissue-level deformations associated with TBI cannot be directly measured *in vivo*, these models can be used to estimate internal brain responses under controlled loading conditions [8–13]. This has been integral to the development of injury criteria and thresholds, in which tissue responses predicted by the models are mapped to head kinematics to establish relationships between external motion and injury risk [11–13]. Several validated FE models of the adult human brain have been developed, most of which are based on a mid-sized adult male representation [14–20]. In contrast, FE brain models for the pediatric population have primarily been developed for infants and young children up to 6 years old [21–25]. Due to the known limitations of scaling adult anatomy to children [26], these pediatric FE brain models are typically derived from pediatric-specific anatomy using age-appropriate computed tomography (CT) or magnetic resonance imaging (MRI) scans or scaled from previously developed pediatric models rather than from adult models. For older children, studies have often relied on adult-derived FE models due to the limited availability of age-specific models [27, 28].

However, the brain undergoes anatomical and biomechanical changes throughout development, including

G Wynn (e-mail: hjn5hk@virginia.edu; tel: (434) 297-8028) is a PhD student in Mechanical and Aerospace engineering, and M.B. Panzer is Professor of Mechanical and Aerospace Engineering at the University of Virginia Center for Applied Biomechanics, Charlottesville, Virginia, USA.

changes in overall size and tissue distribution. Although the pediatric brain nears adult size by early adolescence, grey and white matter volumes follow distinct developmental trajectories, with grey matter peaking in late childhood and white matter increasing into adulthood [29, 30]. Moreover, despite limited literature on the material properties of pediatric brain tissue, existing studies suggest that these properties may differ from those of adults [31–36]. These anatomical and mechanical differences suggest that pediatric brains will respond differently to head impacts than adult brains. Thus, modelling children using adult-based FE models or extrapolating adult injury thresholds to younger populations may be inappropriate. Even if scaling approaches were feasible, injury thresholds may differ between adults and children [37, 38].

The use of existing FE brain models is further complicated by anatomical variability among individuals of the same age. Even under similar impact conditions, different brains may exhibit distinct mechanical responses and injury risks [17, 39–42]. Consequently, relying on a single FE model can overlook individual brain variation. To address the need for models that capture subject-specific anatomies, the Registration-Based Morphing (RBM) framework was developed for rapidly generating subject-specific FE brain models [43]. This RBM pipeline uses the nonlinear transformations produced during the image registration process between a template brain T1-weighted magnetic resonance imaging (MRI) scan and a subject's T1 MRI to morph a template FE model to the subject-specific anatomy. This process produces ready-to-run subject-specific FE brain models that retain accurate neuroanatomical features, including overall size, shape, and localised geometric characteristics, without additional user intervention [43], enabling large-scale investigations into how individual anatomical differences can influence brain deformation during head impact.

This study introduces a new template T1-weighted MRI image and corresponding FE brain model that represents the young adolescent population. The brain model incorporates material properties derived from *in vivo* magnetic resonance elastography (MRE) data from adolescent brain tissue. The template image and model were established to facilitate rapid subject-specific model generation across the pediatric population. This study then used subject-specific models across a diverse population of children to predict how pediatric brain development and aging may affect brain biomechanics from head impact. By improving understanding of pediatric brain biomechanics, this work aims to advance injury prediction and inform the design of protective systems and safety standards tailored to children and adolescents.

METHODS

Model Development

A new pediatric template brain image and FE brain model were developed using the same procedures as those used by Guidice *et al.* [16, 43] for the adult CAB20MSym model. T1-weighted MRI images were obtained from the Adolescent Brain Cognitive Development (ABCD) study [44], which follows the brain growth and development of a diverse sample of youth in the United States. For this study, the dataset was filtered to exclude subjects with neurological or psychiatric conditions, a history of TBI, abnormal brain scans, or other conditions that could affect brain development. The pediatric template brain image was constructed from MRI scans of 120 healthy children spanning six age groups (9–14 years), with 20 scans per age group (10 males and 10 females). Female and male images were combined based on prior findings in adult brains that indicated biological sex was not an independent predictor of brain deformation after accounting for biomechanical and anatomical factors [42].

To create the average pediatric brain anatomy template image, the ANTs multivariate template construction tool [45], an iterative nonlinear registration algorithm, was used. Symmetry was imposed during initial template construction for segmentation and model development efficiency by adding a second image of each subject that was mirrored along the left-right axis to approximate a mid-sagittal reflection. Both the original and mirrored scans (240 total images) were included in the template construction.

The template image was then segmented to associate each voxel with a type of brain tissue. Intracranial volume was first extracted using an automated ANTs brain-extraction script [46], followed by manual corrections to refine brain boundaries and cerebrospinal fluid (CSF) delineation. Tissue segmentation into CSF, white matter (WM), and grey matter (GM) was performed using the ANTs Atropos algorithm with N4 bias-field correction [47], with manual adjustments to ensure accurate tissue classification. The ventricles, sagittal sinus, falx cerebri, and tentorium cerebelli were also manually identified, given their important biomechanical roles [48]. The final template represents the average anatomy of a pediatric population aged 12.0 ± 1.8 years (Fig. 1). The total intracranial volume of the template pediatric brain is 1490 cm^3, the grey matter volume is 751 cm^3, and the white

matter volume is 513 cm^3.

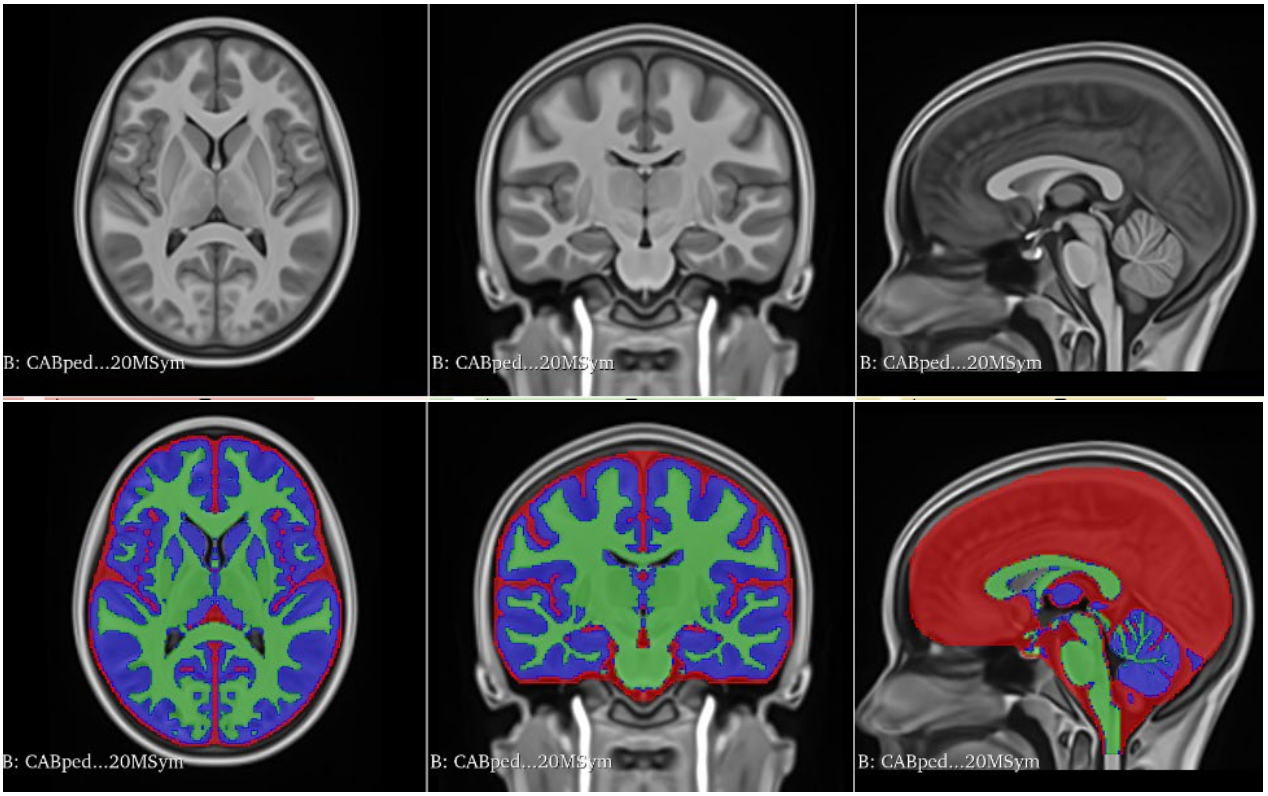

Fig. 1. (Top) final template image that represents the average anatomy of the pediatric brain; (bottom) segmented into white matter (green), grey matter (blue), and cerebral spinal fluid (red) regions

An FE brain mesh was generated from this segmented MRI image by converting each voxel into a cubic hexahedral element using a custom MATLAB script (MathWorks, Natick, MA) (Fig. 2). This voxel-wise meshing preserved the complex anatomical features captured at the native spatial resolution of the MRI data [49]. Each voxel labelled as CSF, GM, or WM in the segmented image was assigned to the corresponding material part within the FE mesh. The sagittal sinus, falx cerebri, and tentorium cerebelli were incorporated by manually adding two-dimensional shell elements at their respective midsurfaces - the sagittal sinus between the brain and skull, the falx between hemispheres, and the tentorium between the cerebrum and cerebellum. To represent the skull-brain interface and enable application of six-degree-of-freedom (6DOF) head kinematics, a rigid shell layer was placed around the peripheral CSF. A simplified version of the adult CAB20MSym model [16, 43] containing the same segmented tissue components served as a reference for baseline comparisons with the new pediatric model. The adult FE model corresponds to an approximately 23-year-old (22.8 ± 3.0 years) male.

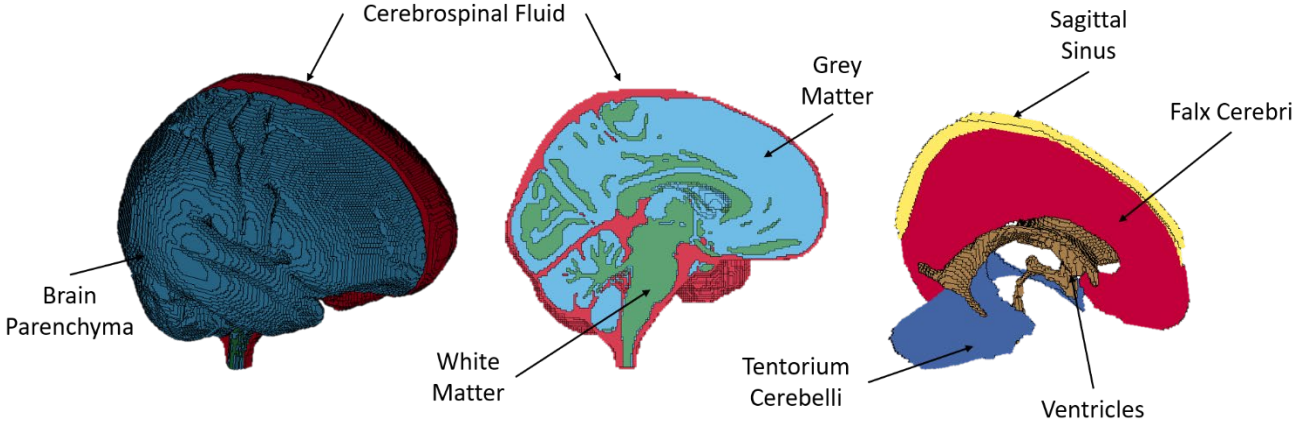

Fig. 2. Components of the pediatric template finite element model

Although data on pediatric brain tissue properties are limited, prior work suggests that the constitutive formulations commonly used for adult brain modelling were also applicable to children; however, the specific material parameters within these equations may differ between age groups [35]. Given the scarcity of pediatric-specific measurements, the present study used the adult CAB20MSym material properties as a baseline and incorporated pediatric-specific modifications where reliable data were available.

Analysis of cerebrospinal fluid (CSF) samples from individuals under 19 revealed viscosities comparable to water, justifying the treatment of pediatric CSF as a Newtonian fluid, consistent with adult modelling [35]. Accordingly, the CSF in the pediatric model was represented identically to that in the adult model. The peripheral CSF was modelled using a low-stiffness linear viscoelastic material (K = 2.1 GPa; G_0 = 0.5 kPa; G_∞ = 0.1 kPa, τ = 0.0125 ms^{-1}) to account for the trabecula and bridging vessels located within the subarachnoid space. The internal CSF and ventricles lack these structures, so they were modelled as an elastic fluid (bulk modulus, K = 2.1 GPa). To the author's knowledge, no data were available on the pediatric properties of the sagittal sinus, falx, or tentorium; thus, these structures were treated as elastic materials (Young's modulus, E = 31.5 MPa; Poisson's ratio, v = 0.45) consistent with the adult model. Finally, the skull was modelled as a rigid body.

Similar to the adult model, the brain parenchyma was modelled as a homogeneous, isotropic tissue using an Ogden-based quasi-linear viscoelastic (QLV) formulation (ρ = 1.123 × 10^{-6} kg/mm^3, ν = 0.499999). The instantaneous elastic response was defined using an incompressible Ogden strain-energy density function (Equation 1), where λ_j are the three principal stretches, μ_i are shear moduli, and α_i are unitless nonlinearity constants, since it has been found to predict the response of brain tissue accurately [50].

$$W(\lambda_1, \lambda_2, \lambda_3) = \sum_{i=1}^{N} \frac{\mu_i}{\alpha_i}\left(\lambda_1^{\alpha_i} + \lambda_2^{\alpha_i} + \lambda_3^{\alpha_i} - 3\right), \quad (1)$$

Viscoelastic behaviour was incorporated through a reduced relaxation function represented by a four-term Prony series, where G_∞ is the long-term shear modulus, G_i are normalised shear stresses, and τ_i are time constants (Equation 2).

$$G(t) = G_\infty + \sum_{i=1}^{N} G_i e^{-\frac{1}{\tau_i}t}, \; G_\infty + \sum_{i=1}^{N} G_i = 1, \quad (2)$$

For the adult model, the reduced relaxation function was calibrated to experimental tan(δ) data describing frequency-dependent damping, and the Ogden parameters were fit to tensile, compressive, and shear testing data [16]. For the pediatric model, these stiffness and viscoelastic parameters were scaled using *in vivo* MRE measurements. McIlvain *et al.* (2022) reported age-related trends in brain stiffness and damping ratio for individuals aged 5–35 years [31]. Global cerebrum properties were used to define pediatric-to-adult scaling relationships for stiffness and viscoelastic damping. Age-dependent stiffness differences were incorporated by multiplying the adult shear modulus by an appropriate scaling factor. Differences in viscoelastic behaviour were accounted for by adjusting the reduced relaxation function. Specifically, the adult tan(δ) curve was scaled using the reported age-specific damping ratio ($\xi = \frac{1}{2}\tan(\delta)$), and the result was refit to determine the pediatric Prony-series coefficients; the time constants from the adult model were retained for the pediatric model.

Based on the linear age-dependent relationship for the storage modulus reported by McIlvain *et al*. (2022) [31], the global cerebrum of a 9-year-old is approximately 5% stiffer than that of a 23-year-old, a 12-year-old is 4% stiffer, and a 14-year-old is 3% stiffer. Thus, the adult elastic modulus was scaled by factors of 1.05, 1.04, and 1.03 for the 9-, 12-, and 14-year-old models, respectively. The resulting stiffness values are reported in Table 2. Conversely, a gradual decrease in the damping ratio with age was reported, with approximately 6% lower damping in 9-year-olds, 5% in 12-year-olds, and 4% in 14-year-olds compared to young adults. To incorporate these trends, the adult tan(δ) curve was scaled by factors of 0.944, 0.956, and 0.964 for the 9-, 12-, and 14-year-old models, respectively, prior to refitting the Prony-series parameters. The resulting scaled G_i coefficients were then applied in the pediatric QLV formulation (Table 1). Because the pediatric template represents a comparable average age, it was assigned the same material properties as the 12-year-old subject group.

TABLE 1
MATERIAL PARAMETERS USED IN THE PEDIATRIC AND ADULT OGDEN QLV CONSTITUTIVE MODELS

	9-Year-Old	12-Year-Old	14-Year-Old	Adult
G_1	0.848	0.851	0.853	0.862
G_2	0.045	0.043	0.042	0.038
G_3	0.042	0.042	0.042	0.041
G_4	0.027	0.027	0.026	0.025
G_∞	0.039	0.038	0.037	0.034
μ (GPa)	4.65	4.60	4.57	4.44

* β_1=10 ms, β_2= 1ms, β_3 = 0.1 ms, and β_4 = 0.01 ms

Subject-specific Model Generation

The developed template brain model was constructed to work with the RBM framework to generate age-specific pediatric FE models. Additional T1-weighted MRI scans were obtained from the same filtered ABCD dataset but from subjects not included in template construction. Six subjects (three male, three female) were selected for each target age group: 9 years (9.0 ± 0.0), 12 years (12.0 ± 0.2), 14 years (14.0 ± 0.11), and 23 years (22.8 ± 0.4). These ages were selected to represent the youngest and oldest children in the ABCD dataset, as well as the average ages corresponding to the pediatric and adult templates.

Each subject's MRI was registered to the appropriate template image (either the new pediatric template or the CAB20MSym adult template) using ANTs [46, 51]. An affine transformation was first applied to align the subject MRI with the template using translation, rotation, scaling, and shear. A nonlinear transformation was then computed to deform the subject MRI voxels to align with the template image. The resulting deformation field was applied to the template FE mesh to map it to each subject's anatomical space, generating subject-specific models for each age group. In total, 24 subject-specific FE brain models were created. The final subject-specific models retain the individual left-right asymmetries introduced by nonlinear registration.

Applying this transformation yielded hexahedral elements that were no longer perfect cubes. Thus, mesh quality was evaluated by computing the scaled Jacobian for each element in every subject-specific mesh. The scaled Jacobian is a standard metric for assessing how much a hexahedral element deviates from an ideal cube. Values of the scaled Jacobian range from -1 to 1, where 1 corresponds to a perfect cube.

Loading Conditions and Simulation Detail

To simulate pediatric brain responses during automotive impacts, exemplar crash-loading conditions were sourced from the literature. The 50th percentile height and weight for children aged 9–14 are 153.1 cm and 46.4 kg, respectively, which is comparable to the 5th percentile female measures (149.8 cm and 49.8 kg) [52]. Thus, head kinematic data from 5th percentile THOR and Hybrid III dummies, as well as 5th percentile female cadaver specimens within 10% of the target child's anthropometric range, were included. Head kinematics from the Gold Standard 2 and 3 sled tests were selected from the National Highway Traffic Safety Administration Biomechanics Test Database [53]. The simulated test conditions involved low-speed (30 km/h) restrained occupants in frontal and oblique orientations. Details on the specific cases are provided in Table 2.

Simulations were performed with LS-DYNA (mpp971R9.1.0, double precision; Livermore Software Technology Corporation, Livermore, CA) on 40 CPUs. All 6-DOF head kinematics (linear acceleration and rotational velocity) were applied to the skull through the head centre of gravity. The numerical approach followed the recommendations of Giudice *et al.*, with all interfaces modelled as continuous and connected via shared nodes [16, 49]. All head kinematics cases were applied to the template models, yielding n=12 per template (1 adult and 1 pediatric template per loading condition). Only a subset of kinematics (n=5, one case per loading direction) were simulated for the subject-specific models (indicated by an asterisk in Table 2). Since each loading condition had to be tested with each subject, one kinematic case per condition was randomly selected, reducing the computational cost from 432 to 180 simulations (30 simulations per age; 6 subjects and 5 loading conditions).

TABLE 2
HEAD KINEMATICS FROM 5TH PERCENTILE FEMALE AUTOMOTIVE CRASH CONDITIONS SIMULATED IN THIS STUDY

Loading condition	Surrogate Type	Case Number	Height (kg)	Weight (m)	PLA (g)	PRA (rad/s^2)	PRV (rad/s)
Gold Standard 2 (GS2)	HIII	S0365*	49.0	149.9	19.1	1369.5	29.1
		S0366	49.0	149.9	15.5	872.8	22.8
	THOR	B12821*	49.0	151.0	20.7	1747.9	30.6
		B12822	49.0	151.0	20.2	1524.5	30.8
	PMHS	B11495*	46.7	151.5	26.4	1524.1	41.6
		B12804	43.6	165.0	23.1	3869.6	44.2
		B12807	46.8	160.0	19.3	1372.7	35.8
Gold Standard 3 (GS3)	THOR	NSFSD0151*	49.0	151.0	36.7	2481.3	38.0
		NSFSD0153	49.0	151.0	25.3	2079.6	38.0
	PMHS	B13162	48.1	154.9	20.7	3209.7	32.8
		B13163	44.4	160.0	22.2	1510.6	34.2
		B13164*	42.6	161.8	24.6	2140.1	33.0

* Subset of kinematics chosen for the subject-specific modelling

** PLA = peak linear acceleration, PRA = peak rotational acceleration, and PRV = peak rotational velocity

Data Analysis

Global brain deformation was quantified using tissue strain, and commonly used metrics were calculated to assess the deformation severity under loading. The maximum principal strain (MPS) was computed for each element throughout the simulation, and the peak value of MPS during the loading event was recorded. The 95th percentile MPS (MPS95) was chosen to avoid potential numerical noise or spurious element effects on the analysis [54]. The cumulative strain damage measure (CSDM) was computed at a threshold of 0.15 to quantify the proportion of brain volume exceeding this strain threshold. MPS95 and CSDM15 values were computed globally across all brain tissues, as well as separately within white matter and grey matter regions.

Our first analysis compared the adult and pediatric templates to assess differences in strain response between the two models across all 12 paired loading conditions. To evaluate the relationship between the pediatric and adult groups as a function of loading severity, linear regression was performed with pediatric response as the predictor and adult response as the outcome. The intercept was set to zero, and the slope was tested against a null hypothesis of equality (slope = 1) to determine proportional scaling.

Our second analysis investigated age-related effects using subject-specific models generated from distinct age-based populations using only a subset of the loading conditions. Strain metrics within each loading case were normalised as the relative difference to the mean adult response of that case to remove the effect of loading severity. To assess whether each age group differed from the adult reference, one-sample t-tests were conducted using the normalised response data against a null value of 0 (indicating equality). The pediatric cohort as a whole was similarly tested against the adult by pooling all normalised pediatric values. All analyses were performed with statistical significance defined as $p < 0.05$.

RESULTS

Adult versus Pediatric Template Model Analysis

The pediatric and adult template models were simulated under matched loading conditions to compare strain outputs. Observed MPS95 values ranged from approximately 0.11 to 0.24, corresponding to a low risk of mild TBI [55]. Overall, the pediatric and adult templates produced highly similar results, with paired responses clustering tightly along the equality line for both the MPS95 and CSDM15 metrics (Figure 3). In general, the variations showed no consistent directional bias; adult models yielded slightly higher values in some regions (e.g., MPS95 GM) and slightly lower values in others (e.g., CSDM15 WM).

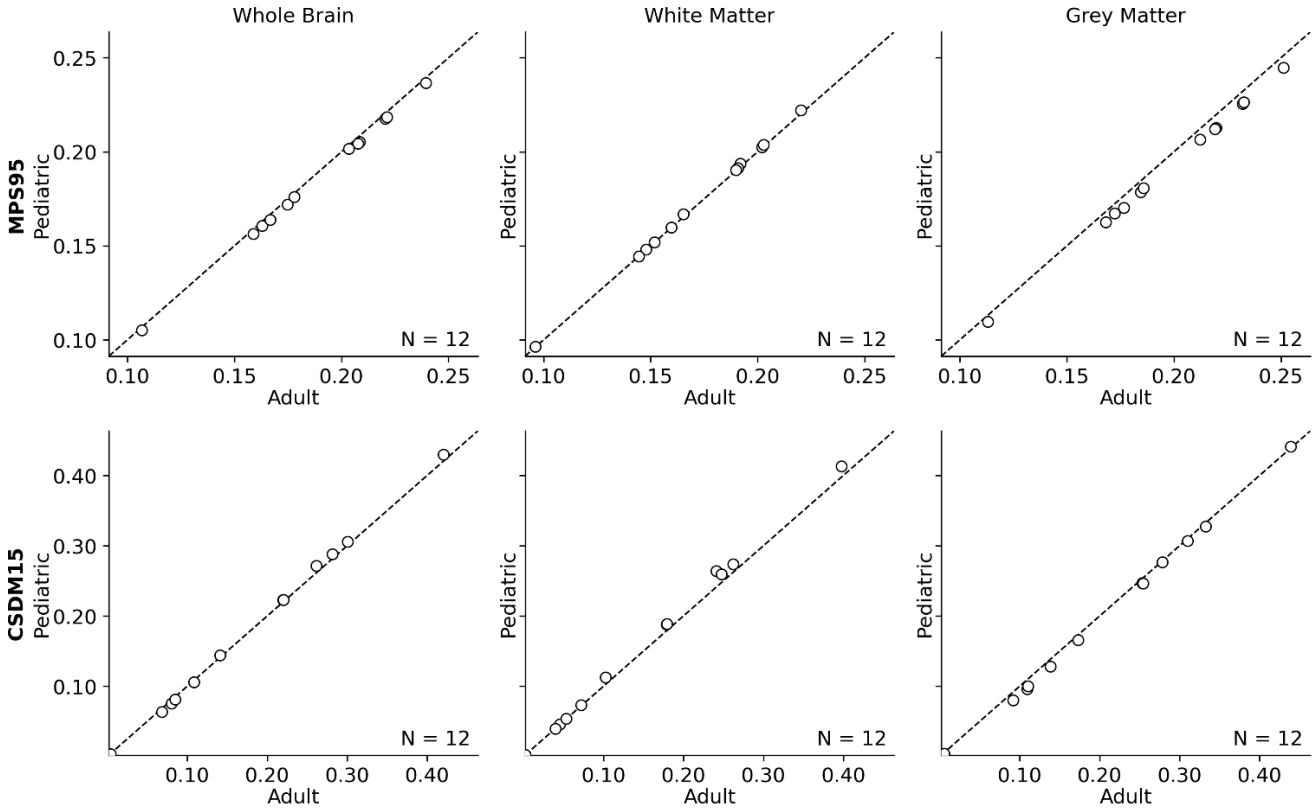

Fig 3. Paired comparisons of pediatric and adult template model responses. Each point represents one test condition with the equality line added as a reference. The close clustering of the data points to the equality line demonstrates minimal differences in strain responses between the two templates.

Differences in MPS95 between the pediatric and adult template models were modest (Table 3). The adult model exhibited slightly higher values across the whole brain (1.3%) and grey matter (2.9%) than the pediatric model, whereas white matter values were nearly identical (<1%). Differences in CSDM15 were only slightly more pronounced but showed different trends than MPS95. Pediatric CSDM15 values were higher in the whole brain (1.9%) and white matter (5.2%) than in the adult brain, but the adult brain had slightly higher CSDM15 values in grey matter (1.7%). While 5 of the 6 model responses were statistically significant ($p < 0.05$), the differences may not be meaningful in the context of injury risk. All regression models produced a fit with $R^2 > 0.99$.

TABLE 3
REGRESSION FOR STRAIN METRICS BETWEEN THE PEDIATRIC AND ADULT TEMPLATE MODELS ACROSS ALL LOADING CONDITIONS

Metric	Tissue	Slope – 1 (%) Mean ±SE
MPS95	All	-1.3 ± 0.1*
	White Matter	0.4 ± 0.1*
	Grey Matter	-2.9 ± 0.1*
CSDM15	All	1.9 ± 0.5*
	White Matter	5.2 ± 0.6*
	Grey Matter	-1.6 ± 0.8

* Indicates $p < 0.05$

The distribution of peak MPS was similar between models, despite subtle differences in the neuroanatomy. Figure 4 illustrates the spatial distribution of peak strain across the simulation for the b13164 kinematic case, which was selected because it yielded the largest MPS95 and CSDM15 responses among all cases.

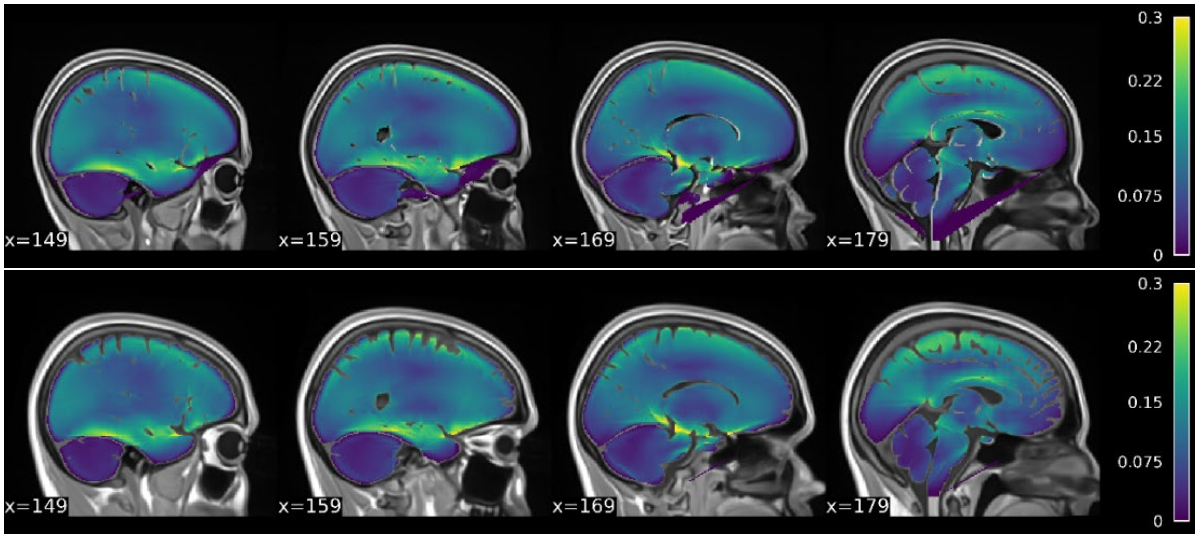

Fig. 4 Sagittal slices depicting peak MPS values distributed onto the pediatric (top) and adult (bottom) template spaces for the b13164 loading condition. The x-coordinates indicate the sagittal slice position relative to the mid-sagittal plane.

Subject-Specific Model Analysis

To expand the assessment of age-related differences beyond the template models, several subject-specific models were generated for each age group. To verify that the RBM method preserved mesh integrity in the subject-specific models, the scaled Jacobian was calculated for each element in each subject-specific model. For the pediatric age-specific models, the median and 95th percentile scaled Jacobians averaged 0.938 ± 0.005 and 0.977 ± 0.002, respectively, and the 5th percentile scaled Jacobian did not fall below 0.849. Adult models demonstrated similarly high quality, with a median of 0.932 ± 0.010, a 95th percentile of 0.976 ± 0.003, and a 5th percentile of 0.834. Thus, RBM maintained excellent mesh quality in morphing the pediatric and adult template models to specific anatomy.

For each simulated loading case, the mean and variance of the subject-specific responses within each age group were evaluated to investigate inter-subject variability and age-related trends. All loading cases showed similar general responses: relative to the adult group, the pediatric groups had slightly higher mean strain metrics and higher inter-subject variability. An example of this trend is shown for the b13164 loading case (Figure 5). The mean responses of MPS95 and CSDM15 were consistent between the 9 and 14-year-old groups, but the 12-year-old cohort exhibited higher peaks and lower variance.

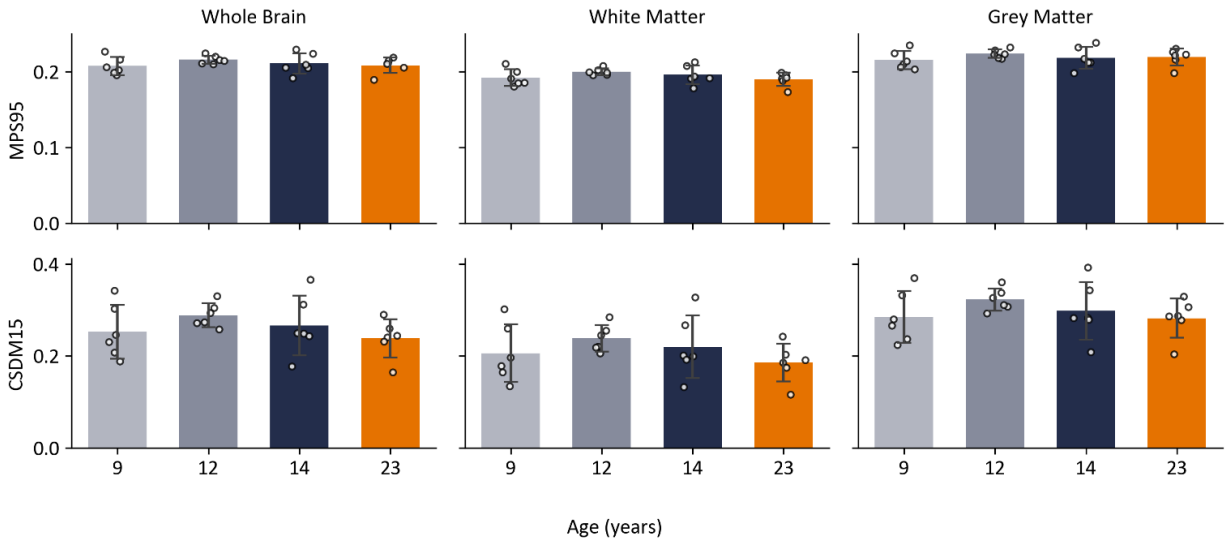

Fig 5. Comparison of MPS95 (top) and CSDM15 (bottom) between each age group across white matter (WM), grey matter (GM), and whole-brain for the b13164 loading condition. Error bars represent one standard deviation from the mean, and circles denote distinct subject-level responses (n=6 per age).

To remove variability due to loading conditions, model responses were normalised to the mean adult metric for each loading case. Differences in normalised strain metrics compared to the adult model were generally positive for both MPS95 and CSDM15 across pediatric groups (Table 4). The pediatric group exhibited a statistically significant increase in MPS95 (4%) and CSDM15 (28%) within the white matter regions compared to the adult group. The increase in strain metrics for the pediatric subjects was largely driven by the 12-year-old cohort, which exhibited significantly higher strain metrics compared to the adults. The responses in the 9- and 14-year-old groups had slightly higher strain metrics relative to the adult group, but these differences were not significant. Furthermore, across the 5-year span of the pediatric group, there was no linear trend between age and strain response (the largest R^2 for the six strain metrics evaluated was 0.26). Variance of responses within the pediatric groups were also observed to be slightly higher than in the adult group.

TABLE 4
NORMALISED STRAIN METRICS ACROSS AGE-SPECIFIC GROUPS, AVERAGED ACROSS ALL LOADING CONDITIONS

		9-Year-Old	12-Year-Old	14-Year-Old	Pediatric
	Tissue	Mean Δ ±SD (%)	Mean Δ ±SD (%)	Mean Δ ±SD (%)	Mean Δ ±SD (%)
MPS95	All	0.3 ± 6.4	4.6 ± 2.6 *	1.7 ± 2.8	2.2 ± 5.9
	WM	1.9 ± 7.2	6.6 ± 2.3 *	3.8 ± 8.0	4.1 ± 6.2 *
	GM	-1.3 ± 6.4	2.8 ± 2.2 *	-0.2 ± 7.4	0.4 ± 5.5
CSDM15	All	7.8 ± 40.5	27.7 ± 12.4 *	14.4 ± 44.2	16.6 ± 33.0 *
	WM	16.4 ± 59.5	40.1 ± 19.4 *	25.8 ± 63.9	27.5 ± 48.0 *
	GM	0.8 ± 30.8	18.5 ± 9.2 *	6.2 ± 34.2	8.5 ± 25.4

* Whole brain (All), white matter (WM), and grey matter (GM)
** SD values represent variability relative to the mean adult strain metric

While the global strain metrics demonstrated confounding results regarding the pediatric response relative to the adult response (and across the pediatric age group), the qualitative assessment of peak MPS distribution revealed subtle differences. Generally, strain was distributed similarly across the adult and pediatric models; however, the adult models exhibited more pronounced strain concentrations along structural interfaces, such as the brain-skull and deep tissue boundaries (Figure 6).

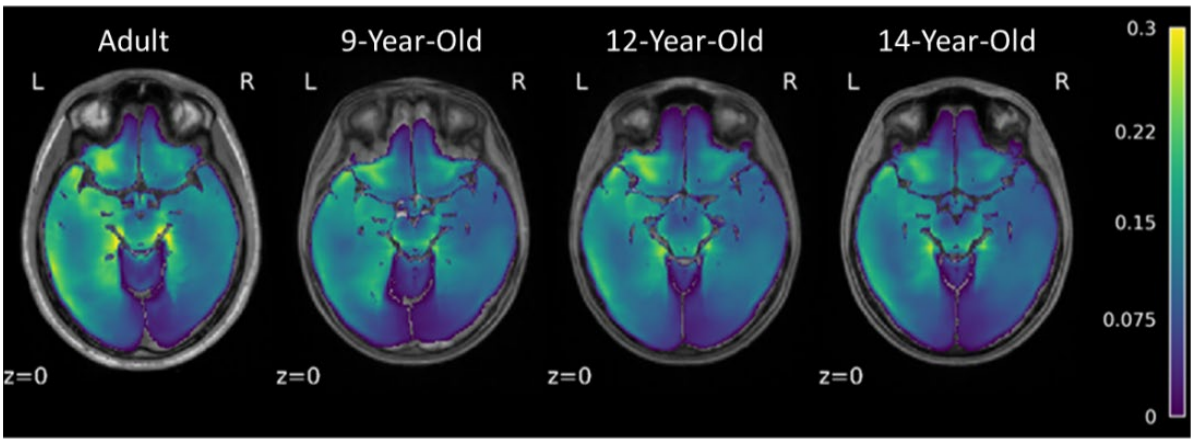

Fig. 6: Representative axial slices display peak MPS values for the adult model alongside the 9-, 12-, and 14-year-old pediatric models for the b13164 exemplar loading case. The z-coordinate indicates the slice position relative to the commissural plane.

DISCUSSION

This study developed anatomically accurate FE models of the pediatric brain and examined age-related differences in brain biomechanics under automotive impact conditions. A pediatric brain template was constructed and integrated into an RBM framework to generate subject-specific pediatric models. This approach addressed known limitations of normalising pediatric neuroanatomy to adult templates, which can lead to tissue

misclassification and excessive deformation during registration [56]. With the template and subject-specific models generated, two distinct analyses were conducted: 1) a template-based comparison utilising generalised FE models to evaluate population-level response differences between pediatric and adult cohorts, and 2) a subject-specific analysis to investigate how individualised anatomy may affect brain deformation outcome beyond the patterns observed in the template-based comparisons.

Model Development

Age-specific material properties were incorporated into the models wherever feasible. Most available pediatric data come from animal studies with immature pigs and rodents, with conflicting trends in stiffness reported in the literature [35]. Studies involving human pediatric brain tissue are scarce. Human brain tissue has been obtained and tested from specimens aged 4–58 years, but age-specific properties were not reported; instead, the authors noted that no statistically significant age differences in stiffness were observed [36]. Only two studies were found that reported age-related differences. One study suggested brain tissue from a 5-year-old was stiffer than that of adults [35], whereas another reported that adult brain tissue was stiffer than that of infants [34]. This uncertainty underscores the need for models that can adapt as new biomechanical data emerge. Within the RBM pipeline, material properties can be easily integrated with new findings, as implemented in this study.

MRE currently offers the most comprehensive in vivo assessment of age-dependent brain properties. The dataset from McIlvain *et al*. (2022) was selected because it spans childhood through adulthood (ages 5-35) and demonstrates trends consistent with adult data from Sack *et al*. [57], who reported a decrease in shear modulus with age (ages 18-88). McIlvain *et al.* observed a global decrease in stiffness and an increase in the damping ratio with age, alongside regional variation and distinct trajectories in grey and white matter [31]. Although some studies report no global mechanical changes during adolescence, they corroborate significant regional and tissue-specific variability [32,33]. Thus, stiffness in the pediatric models was increased by approximately 3–5%, while damping was decreased by 4–6% relative to adult values. One limitation of the current work is that global scaling of stiffness and damping does not capture the full regional heterogeneity observed in developing brains. Future work will leverage spatially varying MRE-derived stiffness maps to introduce regional variation [16].

In addition to limited pediatric material data, the current model development process is limited by the scarcity of pediatric-specific biomechanical data to validate the model response. Ideally, validation efforts would be enabled by available pediatric-tagged MRI and sonomicrometry data, mirroring the validation previously conducted for our adult models [16]. Until validation data become available, pediatric models will need to rely on transferring techniques and approaches from rigorously validated adult models.

Once material properties were defined, all pediatric and adult FE models were simulated under identical automotive loading conditions. To enable direct comparisons between model responses, 5th female percentile head kinematics were simulated in this study. Although the anthropometry of a 5th female is comparable to that of pediatric ages in this study, adult kinematics may not accurately reflect those of adolescents in real-world settings. Studies collecting pediatric head kinematics data using wearable sensors in sports and automotive environments are ongoing and will be valuable contributions to the field.

Analysis of Template Models

Age was a significant predictor of strain when comparing the adult and pediatric template models, but the differences in peak strain between the pediatric and adult template FE models were relatively small, reaching only 3% in the grey matter. Differences in strain distribution were similarly limited, with CSDM15 values differing by no more than 5%. Evaluating the underlying strain distributions overlaid on the brain images, it was evident that the strain patterns are similar despite differences in neuroanatomy between the adult and pediatric template models.

The similarity is likely due to the comparable intracranial volumes (ICVs) of the template models. The total intracranial volume of the pediatric model (1490 cm^3) is only marginally larger than that of the adult template (1440 cm^3). This is similar to other reported pediatric averages [58] and is supported by evidence that brain size typically reaches near-adult dimensions by 10–12 years of age [29,30]. Because previous studies utilising adult models identified ICV as the strongest predictor of deformation metrics like MPS95 and CSDM25 [41,42], it is unsurprising that the pediatric template yielded results similar to those of the adult template. That said, it is premature to conclude that an average adult brain model can be used to simulate pediatric brain injury risk; strain-injury relationships are nonlinear, and the strain differences on the order of 3–5% in the current study may

increase with more severe loading conditions [8,11,59]. Further study is needed to understand the differences in TBI risk between adults and children.

Analysis of Subject-Specific Models

To expand the assessment of age-related differences to a broader population, multiple subject-specific models were developed. Because subject-specific model results depend on accurate morphing, mesh quality was evaluated to confirm the robustness of the RBM approach. Excellent mesh quality was preserved in the subject-specific models, supporting the use of an age-specific template within the RBM pipeline.

As with the template comparisons, the pediatric age group was a significant predictor of strain in the subject-specific analysis, this time showing consistently higher strain in pediatric subjects than in adult subjects. However, this result was largely driven by the 12-year-old cohort, as there were no statistical differences between adults and 9- and 14-year-olds. Although substantial developmental changes occur around this age, it is highly unlikely that 12-year-old neuroanatomy is inherently predisposed to elevated strain levels. The most likely explanation for what was observed in this study is that neuroanatomical variability is greater in the 9- to 14-year-old age range than in adults, and this variability is not easily stratified by chronological age. Furthermore, the confounding results observed in this study will likely be mitigated through additional subject-specific simulations and a deeper investigation into these subjects' morphology.

Nonetheless, there were some interesting findings in the subject-specific analysis that were not apparent in the template model analysis. Differences in CSDM15 were more pronounced when comparing subject-specific models with template models (9-28% vs 2-5%), particularly in white matter regions, where increases in CSDM15 exceeding 30% of adult values were observed. Looking at the exemplar 12-year-old subject compared with the adult subject, both grey and white matter volumes decreased with age (from 770 cm^3 to 636 cm^3 and from 534 cm^3 to 498 cm^3, respectively). Although these trends deviate from well-established population-based patterns of neurodevelopment, where white matter typically increases into adulthood [29,30], they highlight the impact of individual anatomical variation.

These findings align with previous adult studies demonstrating that strain fields can differ substantially between template and subject-specific models [43], and that local brain anatomy and tissue distributions influence the brain deformation response [41,42]. This result emphasises the importance of using individualised anatomy to capture variation. Further, the subject-specific approach revealed distinct strain variations along internal structural boundaries and tissue interfaces across age groups. While the current work does not support definitive conclusions regarding localised regional differences, future studies will incorporate atlas-based brain segmentation to isolate specific anatomical structures, enabling examination of regional biomechanical outcomes across brain development.

Lastly, the higher pediatric strain responses observed in the subject-specific comparisons may also appear counterintuitive given the increased stiffness assigned to pediatric brain tissue, which would be expected to resist deformation more easily. However, these trends may reflect the comparatively lower damping assigned to pediatric models. Because damping governs how deformation energy dissipates over time, reduced damping may permit greater peak strains and a broader spatial extent of moderate strain, contributing to elevated MPS95 and CSDM15 values. This interpretation is supported by prior work comparing male and female brain models, which identified the mean damping ratio as the material parameter with the greatest influence on strain response [60].

Limitations and Future Direction

While this study establishes an anatomically and developmentally informed comparative framework, we must note that the models are not yet validated against pediatric brain deformation data. Our primary objective in this initial study was to evaluate relative differences between adult and pediatric responses by using the same developmental approaches in the pediatric model as were used in the validated adult model. We intend to further enhance the biofidelity of the pediatric model with additional material properties and material heterogeneity from pediatric-specific MRE. Continued progress in the fidelity and analysis of these models is important, as the results of this study demonstrate that subject-specific models are necessary to explicitly evaluate the role of neuroanatomical features in the biomechanics of the pediatric brain and, consequently, the risk of traumatic brain injury. Future analyses will include a deeper assessment of this age range using subject-specific models of pubescent age groups to further explore anatomical effects.

The consistently higher MPS95 and CSDM15 values observed in pediatric subject-specific models indicate an

increased susceptibility to brain deformation, particularly in white matter. These findings suggest that adult FE models may approximate pediatric responses under some conditions, but they may fail to capture developmentally dependent tissue-level deformation patterns critical for injury prediction. Consequently, reliance on global kinematic metrics and criteria developed for adults, such as DAMAGE [9] or BrIC [11], may not adequately capture age-dependent tissue responses. The divergence in pediatric strain patterns under identical head kinematics underscores the need for strain-based injury metrics and tolerance thresholds informed by pediatric-specific anatomy and material behaviour. As pediatric biomechanical data and material properties continue to emerge, incorporating age-specific modelling approaches will be essential to improve pediatric injury prediction and assessment. By pairing anatomically accurate templates with age-informed material properties and subject-specific neuroanatomy, this work provides a framework for examining how developmental factors influence brain strain responses beyond what generalised adult models can capture.

CONCLUSION

This study introduced an FE model of the pediatric brain representing an older child age range, incorporating age-specific anatomy and the best available age-dependent material properties derived from *in vivo* data. By combining an age-appropriate template with subject-specific morphing techniques, the work produced the first anatomically accurate series of 9- to 14-year-old brain models developed using state-of-the-art computational methods. These models captured developmental variability and enabled evaluation of how brain biomechanics evolve during late childhood and early adolescence under realistic automotive loading.

Although global strain metrics suggested similarities between pediatric and adult responses, the results demonstrated that regional differences and evolving neuroanatomy play critical roles in shaping pediatric biomechanical responses. While peak strain metrics (MPS95) were comparable across ages, the subject-specific pediatric models consistently showed greater volumes of moderate strain, particularly in white matter, as reflected in higher CSDM15 values. Adult models also displayed clearer strain distributions along structural interfaces than pediatric models. Differences between pediatric and adult responses were larger and more directionally consistent when individual anatomy was preserved, emphasising the influence of anatomical heterogeneity. Furthermore, individual differences in neuroanatomy within the pediatric cohort led to larger variance in deformation outcomes compared with those observed in adults.

These findings highlight the value of more detailed, region-specific representations of pediatric brain mechanics, as well as the use of age-appropriate loading conditions and material properties as additional data become available. The developed model, in conjunction with the RBM framework, will allow for easy updates and continuous development of these pediatric models. Future work will extend this modelling framework across a broader pediatric age range and integrate spatially heterogeneous MRE-derived stiffness maps.

Ultimately, this research lays the groundwork for a deeper understanding of how brain development shapes injury mechanisms in children. Continued advancement of pediatric FE modelling across diverse ages, neuroanatomies, and loading scenarios will be critical for improving head injury prediction, estimating age-dependent injury thresholds, and informing the design of improved pediatric safety systems.

ACKNOWLEDGEMENTS

We acknowledge the support of the Natural Sciences and Engineering Research Council of Canada (NSERC). Nous remercions le Conseil de recherches en sciences naturelles et en génie du Canada (CRSNG) de son soutien. We also acknowledge Dr. Sebastian Giudice for creating the Registration-Based Morphing framework and assisting with the project formulation.

REFERENCES

[1] Dewan, M.C., Mummareddy, N., *et al.* (2016) Epidemiology of global pediatric traumatic brain injury: qualitative review. *World Neurosurgery*, **91**: pp.497–509.e1.

[2] Dewan, M.C., Rattani, A., *et al.* (2019) Estimating the global incidence of traumatic brain injury. *Journal of Neurosurgery*, **130**(4): pp.1080–1097.

[3] Centers for Disease Control and Prevention. “WISQARS – Web-based Injury Statistics Query and Reporting System”, wisqars.cdc.gov [cited 2025 Dec].
[4] Arbogast, K.B., Durbin, D.R. (2013) Epidemiology of child motor vehicle crash injuries and fatalities. In: Crandall, J.R., Myers, B.S., Meaney, D.F., Zellers Schmidtke, S. (eds.) *Pediatric Injury Biomechanics: Archive & Textbook*, pp.33–86. Springer, New York, NY.
[5] Cunningham, R.M., Walton, M.A., Carter, P.M. (2018) The major causes of death in children and adolescents in the United States. *New England Journal of Medicine*, **379**(25): pp.2468–2475.
[6] Viano, D.C., Parenteau, C.S., *et al.* (2017). Head injuries (TBI) to adults and children in motor vehicle crashes. *Traffic Injury Prevention*, **18**(6): pp.616–622.
[7] Centers for Disease Control and Prevention. (2015) *Report to Congress on Traumatic Brain Injury in the United States: Epidemiology and Rehabilitation*. CDC, Atlanta, GA.
[8] Giordano, C., Kleiven, S. (2014) Evaluation of axonal strain as a predictor for mild traumatic brain injuries using finite element modeling. *Stapp Car Crash Journal*, **58**: pp.29–61.
[9] Gabler, L.F., Crandall, J.R., Panzer, M.B. (2019) Development of a second-order system for rapid estimation of maximum brain strain. *Annals of Biomedical Engineering*, **47**(9): pp.1971–1981.
[10] Sanchez, E.J., Gabler, L.F., *et al.* (2017) Evaluation of head and brain injury risk functions using sub-injurious human volunteer data. *Journal of Neurotrauma*, **34**(16): pp.2410–2424.
[11] Takhounts, E.G., Craig, M.J., *et al.* (2013) Development of brain injury criteria (BrIC). *SAE Technical Paper*, 2013-22-0010.
[12] Takhounts, E.G., Ridella, S.A., *et al.* (2008) Investigation of traumatic brain injuries using the next generation of simulated injury monitor (SIMon) finite element head model. *SAE Technical Paper*, 2008-22-0001.
[13] Rowson, S., Duma, S.M. (2013) Brain injury prediction: assessing the combined probability of concussion using linear and rotational head acceleration. *Annals of Biomedical Engineering*, **41**(5): pp.873–882.
[14] Ji, S., Zhao, W., *et al.* (2015) Group-wise evaluation and comparison of white matter fiber strain and maximum principal strain in sports-related concussion. *Journal of Neurotrauma*, **32**(7): pp.441–454.
[15] Takhounts, E.G., Eppinger, R.H., *et al.* (2003) On the development of the SIMon finite element head model. *SAE Technical Paper*, 2003-22-0007.
[16] Giudice, J.S., Alshareef, A., *et al.* (2021) Calibration of a heterogeneous brain model using a subject-specific inverse finite element approach. *Frontiers in Bioengineering and Biotechnology*, **9**: 664268.
[17] Li, X., Zhou, Z., Kleiven, S. (2021) An anatomically detailed and personalizable head injury model: significance of brain and white matter tract morphological variability on strain. *Biomechanics and Modeling in Mechanobiology*, **20**(2): pp.403–431.
[18] Wu, T., Alshareef, A., *et al.* (2019) Explicit modeling of white matter axonal fiber tracts in a finite element brain model. *Annals of Biomedical Engineering*, **47**: pp.1908–1922.
[19] Atsumi, N., Nakahira, Y., Iwamoto, M. (2016) Development and validation of a head/brain finite element model and investigation of influential factors on the brain response during head impact. *International Journal of Vehicle Safety*, **9**(1): pp.1–23.
[20] Mao, H., Zhang, L., *et al.* (2013) Development of a finite element human head model partially validated with thirty five experimental cases. *Journal of Biomechanical Engineering*, **135**: p.111002.
[21] Li, Z., Hu, J., *et al.* (2011) Development, validation, and application of a parametric pediatric head finite element model for impact simulations. *Annals of Biomedical Engineering*, **39**(12): pp.2984–2997.
[22] Roth, S., Raul, J.-S., Willinger, R. (2010) Finite element modelling of paediatric head impact: global validation against experimental data. *Computer Methods and Programs in Biomedicine*, **99**(1): pp.25–33.
[23] Wilhelm, J., Ptak, M., *et al.* (2020) Injury biomechanics of a child’s head: problems, challenges and possibilities with a new aHEAD finite element model. *Applied Sciences*, **10**(13): p.4467.
[24] Giordano, C., Li, X., Kleiven, S. (2017) Performances of the PIPER scalable child human body model in accident reconstruction. *PLOS ONE*, **12**(11): e0187916.
[25] Cui, S., Li, H., *et al.* (2015) Effects of the variation in brain tissue mechanical properties on the intracranial response of a 6-year-old child. *Computational and Mathematical Methods in Medicine*, **2015**: 529729.
[26] Roth, S., Raul, J.-S., *et al.* (2007) Limitation of scaling methods in child head finite element modelling. *International Journal of Vehicle Safety*, **2**(4): pp.404–421.
[27] Le, M., Je, U., *et al.* (2019) Evaluation of brain response during head impact in youth athletes using an anatomically accurate finite element model. *Journal of Neurotrauma*, **36**(10): pp. 1561–1570.

[28] Dawson, L., Koncan, D., *et al.* (2020) Biomechanical comparison of real world concussive impacts in children, adolescents, and adults. *Journal of Biomechanical Engineering*, **142**(7): p.071004.
[29] Giedd, J.N., Raznahan, A., *et al.* (2012) Review: magnetic resonance imaging of male/female differences in human adolescent brain anatomy. *Biology of Sex Differences*, **3**(1): p.19.
[30] Bethlehem, R.A.I., Seidlitz, J., *et al.* (2022) Brain charts for the human lifespan. *Nature*, **604**(7906): pp.525–533.
[31] McIlvain, G., Schneider, J.M., *et al.* (2022) Mapping brain mechanical property maturation from childhood to adulthood. *NeuroImage*, **263**: p.119590.
[32] McIlvain, G., Schwarb, H., *et al.* (2018) Mechanical properties of the in vivo adolescent human brain. *Developmental Cognitive Neuroscience*, **34**: pp.27–33.
[33] Yeung, J., Jugé, L., *et al.* (2019) Paediatric brain tissue properties measured with magnetic resonance elastography. *Biomechanics and Modeling in Mechanobiology*, **18**(5): pp.1497–1505.
[34] Chatelin, S., Vappou, J., *et al.* (2012) Towards child versus adult brain mechanical properties. *Journal of the Mechanical Behavior of Biomedical Materials*, **6**: pp.166–173.
[35] Margulies, S., Coats, B. (2013) Experimental injury biomechanics of the pediatric head and brain. In: Crandall, J.R., Myers, B.S., Meaney, D.F., Zellers Schmidtke, S. (eds.) *Pediatric Injury Biomechanics*, pp.157–189. Springer, New York, NY.
[36] Basilio, A.V., Zeng, D., *et al.* (2024) Region-dependent mechanical properties of human brain tissue under large deformations using inverse finite element modeling. *Annals of Biomedical Engineering*, **52**(3): pp.600–610.
[37] Campolettano, E.T., Gellner, R.A., *et al.* (2020) Development of a concussion risk function for a youth population using head linear and rotational acceleration. *Annals of Biomedical Engineering*, **48**(1): pp.92–103.
[38] Rowson, B., Duma, S.M. (2020) A review of on-field investigations into the biomechanics of concussion in football and translation to head injury mitigation strategies. *Annals of Biomedical Engineering*, **48**(12): pp.2734–2750.
[39] Giordano, C., Zappalà, S., Kleiven, S. (2017) Anisotropic finite element models for brain injury prediction: the sensitivity of axonal strain to white matter tract inter-subject variability. *Biomechanics and Modeling in Mechanobiology*, **16**: pp.1269–1293.
[40] Rifkin, J.A., Wu, T., *et al.* (2022) Brain architecture-based vulnerability to traumatic injury. *Frontiers in Bioengineering and Biotechnology*, **10**: 936082.
[41] Giudice, J. S.; Druzgal, T. J.; *et al.* (2023). Investigating the Effect of Brain Size on Deformation Magnitude Using Subject-Specific Finite Element Models, *Journal of Neurotrauma*, **40**: pp. 1796–1807.
[42] Reynier, K. A.; Giudice, J. S., *et al.* (2022). Quantifying the Effect of Sex and Neuroanatomical Biomechanical Features on Brain Deformation Response in Finite Element Brain Models, *Annals of Biomedical Engineering*, **50**(11): pp.1510–1519.
[43] Giudice, J.S., Zeng, W., *et al.* (2020) An image registration-based morphing technique for generating subject-specific brain finite element models. *Annals of Biomedical Engineering*, **48**(10): pp.2412–2424.
[44] Casey, B.J., Cannonier, T., *et al.* (2018) The adolescent brain cognitive development (ABCD) study: imaging acquisition across 21 sites. *Developmental Cognitive Neuroscience*, **32**: pp.43–54.
[45] Avants, B.B., Yushkevich, P., *et al.* (2010) The optimal template effect in hippocampus studies of diseased populations. *NeuroImage*, **49**(3): pp.2457–2466.
[46] Avants, B.B., Tustison, N.J., *et al.* (2011) A reproducible evaluation of ANTs similarity metric performance in brain image registration. *NeuroImage*, **54**(3): pp.2033–2044.
[47] Avants, B.B., Tustison, N.J., *et al.* (2011) An open source multivariate framework for n-tissue segmentation with evaluation on public data. *Neuroinformatics*, **9**(4): pp.381–400.
[48] Ho, J., von Holst, H., Kleiven, S. (2009) Automatic generation and validation of patient-specific finite element head models suitable for crashworthiness analysis. *International Journal of Crashworthiness*, **14**(6): pp.555–563.
[49] Giudice, J.S., Zeng, W., *et al.* (2019) An analytical review of the numerical methods used for finite element modeling of traumatic brain injury. *Annals of Biomedical Engineering*, **47**(9): pp.1855–1872.
[50] Budday, S., Sommer, G., *et al.* (2017) Mechanical characterization of human brain tissue. *Acta Biomaterialia*, **48**: pp.319–340.

[51] Avants, B.B., Epstein, C.L., *et al.* (2008) Symmetric diffeomorphic image registration with cross-correlation: evaluating automated labeling of elderly and neurodegenerative brain. *Medical Image Analysis*, **12**(1): pp.26–41.
[52] Fryar, C.D., Carroll, M.D., *et al.* (2025) *Anthropometric Reference Data for Children and Adults: United States, 2015–2018*. National Center for Health Statistics, Hyattsville, MD.
[53] National Highway Traffic Safety Administration. "Biomechanics Test Database", www.nhtsa.gov/research-data/research-testing-databases.
[54] Panzer, M.B., Myers, B.S., *et al.* (2012) Development of a finite element model for blast brain injury and the effects of CSF cavitation. *Annals of Biomedical Engineering*, **40**(7): pp.1530–1544.
[55] Wu, T., Hajiaghamemar, M., *et al.* (2021) Evaluation of tissue-level brain injury metrics using species-specific simulations. *Journal of Neurotrauma*, **38**(13): pp.1879–1888.
[56] Sanchez, C.E., Richards, J.E., Almli, C.R. (2012) Age-specific MRI templates for pediatric neuroimaging. *Developmental Neuropsychology*, **37**(5): pp.379–399.
[57] Sack, I.; Beierbach, B., *et al.* (2009). The impact of aging and gender on brain viscoelasticity, *NeuroImage*, **46**(3): pp. 652–657.
[58] Richards, J. E.; Sanchez, C.; Phillips-Meek, M.; Xie, W. (2016). A database of age-appropriate average MRI templates, *NeuroImage*, Vol. 124, No. Pt B, 1254–1259. doi:10.1016/j.neuroimage.2015.04.055
[59] Zhan, X., Li, Y., *et al.* (2021) The relationship between brain injury criteria and brain strain across different types of head impacts can be different. *Journal of the Royal Society Interface*, **18**(179): 20210260.
[60] Reynier, K. (2022). *Quantifying the Effect of Sex-Related Differences in Biomechanical Factors on Brain Deformation Response.* PhD Dissertation. University of Virginia.